

# Eyes on the Prize: Improved Registration via Forward Propagation

Robert Ravier<sup>1</sup>

<sup>1</sup>Department of Electrical and Computer Engineering, and Department of Mathematics,  
Duke University

June 29, 2022

## Abstract

We develop a robust method for improving pairwise correspondences for a collection of shapes in a metric space. Given a collection  $f_{ji} : S_i \rightarrow S_j$  of correspondences, we use a simple metric condition, which has a natural interpretation when considering the analogy of parallel transport, to construct a Gibbs measure on the space of correspondences between any pair of shapes that are generated by the  $f_{ji}$ . We demonstrate that this measure can be used to more accurately compute correspondences between feature points compared to currently employed, less robust methods. As an application, we use our results to propose a novel method for computing homeomorphisms between pairs of shapes that are similar to one another after alignment.

## 1 Introduction

The shape registration problem is one of utmost importance in computer graphics, statistical shape analysis, and other fields. Specifically, given two shapes  $S_i$  and  $S_j$  embedded in Euclidean space, we would like to compute a high-quality correspondence  $f_{ji} : S_i \rightarrow S_j$  between the shapes; the desired level of regularity of  $f_{ji}$  ultimately depends on user interest. There has been substantial effort devoted to this problem in recent years; see, for example, [1, 2, 13–15, 24–26, 28, 33, 36, 40], though note our list is by no means exhaustive. In particular, the work in [1, 2, 36] give possible solutions for shapes that are represented by surfaces provided that prescribed landmark correspondences are known and the underlying surfaces have non-disk topology. Other methods that do not depend pre-established landmarks also exist, including [24, 26, 28, 40].

For the purposes of performing comparative analyses of collections shapes, merely computing pairwise registrations is insufficient. We also require that the computed pairwise mappings be *consistent*. Specifically, we require that all registrations between shapes  $A$  and  $B$  generated by composition of the individual pairwise registrations be equal to one another. Figure 1 gives an example of a collection of maps being inconsistent. Consistent maps allow us to have well-defined references to given points and regions on a shape, and thus allow us to perform comparative analysis of shapes. Inconsistent maps, on the other hand, create ambiguity that prevents such analysis. The problem of extracting a consistent collections of correspondences from a given initial collection has received significant attention. Joint segmentation can be viewed as a variant of this problem, and the problem for discrete pointwise maps has been studied in [20, 21] via semidefinite programming, similar to studies of other synchronization problems [3, 9, 37].

A naive yet natural way to make a collection of mappings consistent is via the extraction of spanning trees, as in [1, 8, 32]. We can represent a collection of shapes and pairwise correspondences via a graph, where each shape is represented by a vertex and each pairwise correspondence is represented by an edge between two vertices. It is an easy exercise to show that all consistent collections of registrations (and,

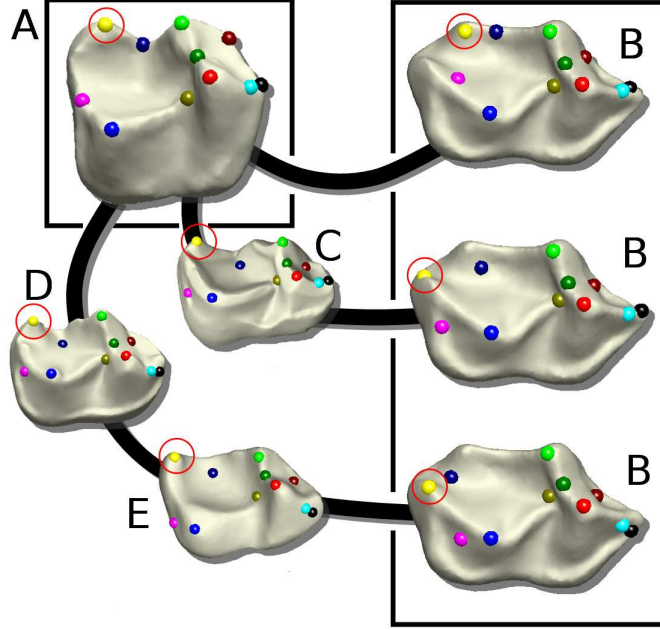


Figure 1: Different correspondences between surfaces  $A$  and  $B$ , visualized via colored landmarks. Each pairwise correspondence is computed via the algorithm in [28]. The lower two correspondences, generated by composing pairwise correspondences along intermediaries, differ from the top pairwise correspondence, as can be seen by looking at the position of the circled landmarks

more generally, transformations) are inherently born out of the structure of a spanning tree; the consistency is a direct consequence of the fact that there is only one path up to backtracking between any two vertices in a spanning tree. There are, however, a plethora of issues brought up by extracting spanning trees. For example, while spanning trees will force consistency, there is no underlying guarantee of accuracy. In general, the problem of finding the optimal spanning tree of such a graph is NP-hard (see [22]), leaving little hope without more assumptions. Even with a well-defined heuristic for choosing a spanning tree, though, we still have the issue of how spanning trees attempt to make a collection consistent. Unlike optimization-based methods, which utilize all of the information present from the initial computation in order to compute refined mappings, tree-based methods utilize some heuristic to pare down the graph until it is a spanning tree. Depending on the method for constructing the tree from the graph, this can lead to a plethora of undesirabilities. If the graph contains multiple valid registrations between two shapes, represented by different paths in the graph, the pruning process inevitably chooses only one of these transformations, leaving out perfectly good information in name of a choice. This is in stark contrast to methods based in optimization, which essentially attempt to blend the information from all of the registrations together in order to compute something new. Furthermore, if one of the pairwise registrations corresponding to a chosen edge of the tree is inaccurate, then many of the other tree-refined transformations can also be bad depending on the location of the edge of the tree in the graph.

The 2013 dissertation of Jesus Puente and subsequent work suggests using a minimum spanning tree (MST) approach deployed in the software package Auto3DGM [8, 32]. The MST heuristic is motivated by experimental evidence suggesting a positive correlation between correctness of transformations and small distances between shapes in a metric space; intuitively, point clouds that are closer to one another are more

likely to have similar geometric features, which makes accurate registrations more attainable. The MST uses these shape distances in order to choose what edges of the graph are used

The MST replaces registrations between shapes of larger distance with transformations constructed by composing maps along paths in the graph over numerous edges of smaller weight. Despite the potential for numerical error due to the possibly large number of compositions needed to map and align the point clouds, the algorithm still tends to produce accurate result. The MST-based approach of Auto3DGM exhibits similar behavior in the context of the similar yet distinct continuous Procrustes distance (CPD) [28], where the point clouds are replaced by smooth surfaces (represented computationally as triangular meshes) and the permutations are replaced with area preserving diffeomorphisms. Here, the underlying graph structure present in the problem allows the ability to handle the diffeomorphisms without a problem, as the resulting consistent mapping constructed between any pair of surfaces is created by composing compatible maps with one another. In this example, while the optimization is over a space of mappings whose structure is unknown, one can prove that, for two surfaces with sufficiently small CPD, the resulting map can be well-approximated by a conformal map, the space of which is easy to search over via brute force, giving additional credence to the choice of a minimum spanning tree as a way to create the synchronized maps. Indeed, the same behavior regarding the accuracy of transformations from the GPD was observed with those from the CPD, see Figure 1 and [18].

There are issues with the MST-based approach that brings its long-term viability into question. Aside from the previously described issues of using spanning trees to synchronize in general, MSTs suffer from instability of topology in the following sense: the MST corresponding to a collection of specimens may become wildly different in shape upon adding or removing specimens from the collection. Figure 2 gives an example of this occurring on a collection of tooth crown surfaces. Given that the correlation between small distances and quality of transformations is not completely one to one, this yields significant potential for instability in the resulting synchronization process, a trait that has already been observed in another context in [42].

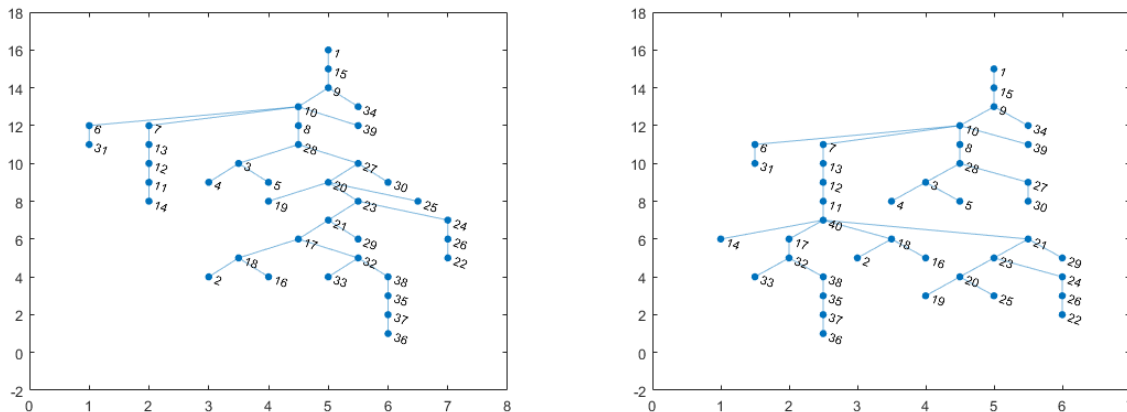


Figure 2: Top: topology of the MST obtained by computing the Continuous Procrustes Distance on 39 teeth from the dataset used in [7]. Right: topology of the MST obtained by adding one specimen (labeled 40) to the dataset used in constructing the tree on the top. Note the substantial difference in connectivity structure

The main goal of this work is to construct and test a new method that addresses this instability while still maintaining the major observed benefits of the MST-based approach. We will specifically focus on

robustly improving pairwise correspondences, from which we can constrain consistency via the use of a tree. To design our correspondence improvement, we first observe that Auto3DGM and other tree-based synchronization methods can be viewed as a special case of a more general probabilistic framework if we relax the assumption that we are interested in explicit transformations, but rather *distributions* of correspondences, as is done in the soft maps framework [39]. With this in mind, we see that if we could construct good distributions on the space of maps of interest, we could then take some projection the distributions to some element of the space of interest by taking a Frechet mean or some other statistic of interest; the observation in Figure 1 supports this notion.

The desire to favor paths consisting of traversing edges of smaller weight gives a natural candidate as to how to weigh the maps corresponding to a given path in the graph  $\Gamma$ . Nevertheless, an appropriate choice of weights is not enough in order to properly define a distribution. Without any assumption on the consistency of correspondences (which would render this problem moot as every distribution would be a delta), we must be careful insofar as whether we use the transformation corresponding to a given path whatsoever in constructing our distributions. This is where the issue of *holonomy*, as discussed in [14–16] comes into play. The map corresponding to any path with a loop should clearly have zero weight, as any such transformation can be thought of as one coming from a simple path that was perturbed by the loop and the lack of consistency. Even then, as we will see, simply not weighting paths with loops is not enough; from a manifold learning perspective, the underlying curvature of the manifold induces its own error when composing correspondences along paths. We will ultimately address this by creating *directed* graph cuts that are constructed by making use of the metric space structure. Our method of addressing is somewhat analogous to the idea behind directed diffusion networks [23], though ours make use of metric structure not present in this model.

The rest of the chapter is outlined as follows. In section 2, we outline both intuition and precise definitions concerning our paradigm, dubbed *eyes on the prize*, which only allows paths that always move away from their source and towards their target. This is further elaborated on in the Appendix, where we investigate a theoretical analogue of the mapping problem in Riemannian geometry, the problem of parallel transporting along a geodesic, and show that our algorithm yields a natural interpretation as a robust approach on this problem. In Section 3, we detail algorithms to robustify the correspondence procedure, and then propose a more robust method to making correspondences consistent. In Section 4, we outline an application of our algorithms to develop a method to register similar shapes by refining alignments. In Section 5, we make concluding remarks.

## 2 Defining a Distribution on the Space of Correspondences

### 2.1 Notation

In the sequel, we will let  $\mathcal{X}$  be a finite collection of shapes embedded in a metric space. For any two shapes  $X, Y \in \mathcal{X}$ , we let  $C_{Y,X}$  be some class of mappings from  $X$  to  $Y$ . We let  $\Gamma = (V, E)$  be a connected graph with  $n$  vertices such that vertex  $v_i$  corresponds to  $X_i$  and an edge between  $v_i$  and  $v_j$  corresponds to two pairs  $(d_{ji}, f_{ji})$  and  $(i_j, f_{ij})$ , where the  $d_{ji}$  are some notion of distance (e.g. continuous Procrustes) between  $X_i$  and  $X_j$ . and  $f_{ji} = f_{ij}^{-1} \in C_{X_j, X_i}$  are maps that are computed in determining the distance. We will sometimes refer to  $\Gamma$  as a *synchronization graph*. We will also let  $C(v_i, v_j)$  be the space of paths on  $\Gamma$  between  $v_i$  and  $v_j$ , where we represent the specific elements by finite sequences  $(a_1, \dots, a_k)$  of numbers in  $\{1, \dots, n\}$ , where  $a_1 = i$  and  $a_k = j$ . Given a path  $\gamma = (a_1, \dots, a_k) \in C(v_i, v_j)$ , we let  $f_\gamma \in C_{X_j, X_i}$  be defined by

$$f_\gamma = f_{a_k a_{k-1}} \circ \dots \circ f_{a_2 a_1}, \quad (1)$$

and we define the function  $\mathcal{G}_{ji} : C(v_i, v_j) \rightarrow C_{X_j, X_i}$  by

$$\mathcal{G}_{ji}(\gamma) = f_\gamma. \quad (2)$$

## 2.2 Holonomy-Inspired Motivation

Given a complete graph  $\Gamma = (V, E)$  with  $|V| = n > 2$ , corresponding shapes  $S_1, \dots, S_n$  edge weights  $d_{ji}$ , and correspondences  $f_{ji}$  as outlined in the previous subsection, we would like to define a distribution on the collection of maps between any two shapes generated by paths between corresponding vertices on the graphs that favor composing maps between pairs of shapes with small distances. A natural choice for this, for shapes  $S_i$  and  $S_j$  is to take the Gibbs measure

$$\mathbb{P}(f_\gamma) \propto e^{-\beta E(\gamma)}, \quad (3)$$

where  $\beta$  is some parameter and  $E(\gamma)$  for  $\gamma = (v_1, \dots, v_k)$  is an energy function defined by

$$E(\gamma) := \sum_{m=1}^{k-1} d_{v_{m+1}v_m}^2 \quad (4)$$

In general, even if we exclude all such  $\gamma$  that have a subsequence of the form  $(a, b, a)$ , i.e. all backtracking paths, we are still in general left with a measure of infinite support, which would require the use of sampling algorithms, such as Metropolis-Hastings, if we wanted to sample from this distribution.

However, given the presumed lack of consistency of the mappings, it is not ideal to keep every correspondence in the support of this distribution. To see why, we consider the case of a correspondence generated by a path  $\gamma$  containing a single loop at some vertex  $v_k$ , and the path  $\tilde{\gamma}$  with the loop erased. If the maps were consistent, the map generated by the loop in  $\gamma$  would simply be the identity on  $S_k$ . In this case we would have  $f_\gamma = f_{\tilde{\gamma}}$ . Given that they are inconsistent, the map generated by the loop is not the identity in general. We can thus think of  $f_\gamma$  as  $f_{\tilde{\gamma}}$  with some error perturbation caused by the loop. Ideally, we should simply omit all such maps corresponding to paths with loops from the support of the distribution. This greatly improves our ability to sample, as the support of the distribution is now no longer infinite; the support is now the maps generated by the simple paths between  $v_i$  and  $v_j$ . For many practical cases, where correspondences and distances are known for every pair of shapes in a collection, this is still too impractically large as the number of such simple paths in this case is  $n!$  with notation given above. If possible, we should further reduce the support of the measure.

In order to better understand how one could do this, we now appeal to geometry. In his dissertation, Gao proposed the notion of the fibre bundle assumption, a specific case of the manifold assumption where the individual data points are assumed to have enough structure such that the data points themselves can be viewed as manifolds; the total manifold is thus a fibre bundle [14, 15]. We refer the interested reader to these works for specific details. The main detail that we use is, under this assumption, correspondences have a natural interpretation as *parallel transports* on a manifold. We defer a precise definition of parallel transport to the appendix, though roughly speaking, parallel transports are isomorphisms of tangent spaces based at different points on a manifold obtained as the solution of some differential equation with respect to a particular curve between those two points.

Parallel transports also in general suffer from the same inconsistency as correspondences. To see this, consider Figure 3, where we illustrate an example of this. For  $S^2$ , we consider the parallel transport of a vector  $v \in T_P M$  to vectors in  $T_Q M$  by parallel transporting along two different paths: one by parallel transporting along the geodesic between  $P$  and  $Q$ , and another by parallel transporting along the geodesic between  $P$  and  $R$  followed by the geodesic from  $R$  to  $Q$ , where  $R$  is one of the poles of  $S^2$  corresponding

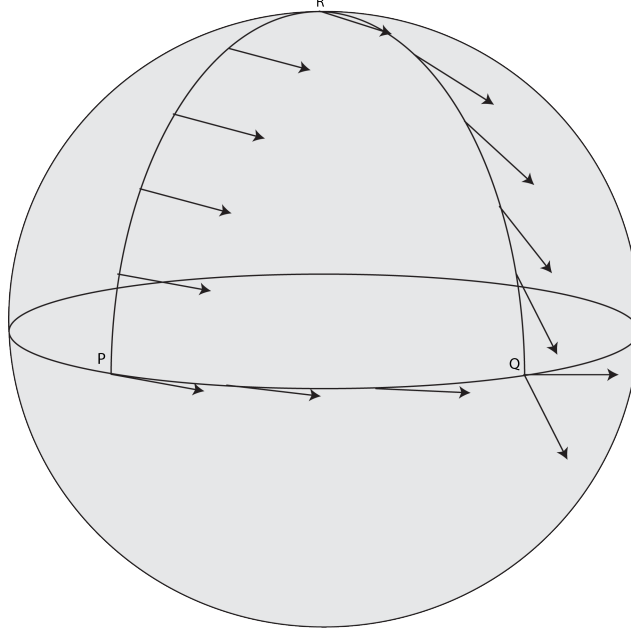


Figure 3: Two parallel transports of a tangent vector at a point  $P$  on  $S^2$ . One transport follows along two sides of a geodesic triangle to a point  $Q$ , while the other transport follows the geodesic between  $P$  and  $Q$ .

to the great circle connecting  $P$  and  $Q$ . It is clear that the resulting parallel transports are quite different. This happens in general for other manifolds; specifically, the region enclosed by the corresponding geodesic triangle generated by the two curves contains enough curvature to distort the parallel transport of the non-geodesic curve relative to the geodesic, a fact we also make more precise in the Appendix.

A common, reasonable assumption (GET CITATIONS) in the field of shape registration is that good correspondences can be obtained by following geodesics in shape space. If we keep this assumption, then the discussion in the above paragraph gives us a potential way forward: the support of our distribution should only contain paths that have some discernable performance guarantee relative to the geodesic, which we usually do not know a priori.

### 2.3 Eyes on the Prize: A Directed Diffusion Condition

Let  $D = (d_{ij})$  is the matrix of computed distances between every shape in the collection in the previous subsection.

**Definition 1.** For vertices  $v_i$  and  $v_j$  in a connected weighted graph  $\Gamma = (V, E)$  with edge weights given by a matrix  $D = (d_{ij})$  with  $d_{ij} = d(v_i, v_j)$  for some metric  $d$ , we define the **directed flow matrix between  $v_i$  and  $v_j$** , denoted by  $F_{i \rightarrow j}^\Gamma$ , is the  $|V| \times |V|$  binary matrix defined by

$$(F_{i \rightarrow j}^\Gamma)_{mn} := \begin{cases} 1 & \text{if } d(v_i, v_m) < d(v_i, v_n) \text{ and } d(v_j, v_m) > d(v_j, v_n) \\ 0 & \text{otherwise} \end{cases} \quad (5)$$

From this, we can define a directed subgraph  $\tilde{\Gamma}_{ij}$  of  $\Gamma$  by taking the adjacency matrix of  $\tilde{\Gamma}$  to be  $D * F_{i \rightarrow j}^\Gamma$ , where  $*$  denotes the entrywise Hadamard matrix product. Intuitively, a directed edge is in this graph only if by going along a directed edge, we move further away from  $v_i$  and closer to  $v_j$ . Given this behavior, we sometimes denote the matrix in 2.3 as the *eyes on the prize* matrix between  $v_i$  and  $v_j$ .



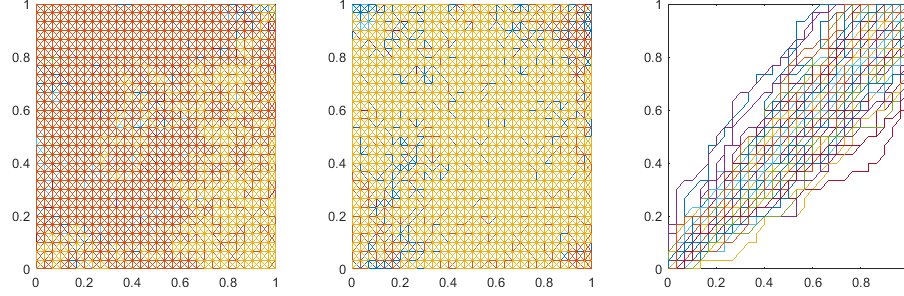


Figure 4: Walks on a  $31 \times 31$  lattice on the unit square. Left: Three walks generated by the standard unweighted random walk. Center: Three generated by the nonbacktracking matrix. Right: One hundred walks generated by the eyes on the prize matrix.

The major qualitative properties can be visualized when we treat  $F_{i \rightarrow j}^\Gamma$  as an unnormalized, close to Markov matrix (it is not Markov as any walk dies at  $j$ ), and look at the random paths from  $i$  to  $j$  that are generated. We compare the paths generated by  $F_{i \rightarrow j}^\Gamma$  to those generated by two other common adjacency structures: the standard (unweighted) adjacency matrix  $A$  and the Hashimoto non-backtracking matrix used in the study of belief propagation, a matrix which allows for all walks except for those of the form  $i \rightarrow j \rightarrow i$  [5, 19, 35, 38]. Figure 4 shows the difference between the eyes on the prize walk and walks generated by an adjacency and nonbacktracking matrix. We specifically consider a  $31 \times 31$  lattice on the unit square, with the points on each row and column equispaced. The connectivity structure we place on the graph says that each vertex is connected to its immediate horizontal, vertical, and diagonal neighbors. In the figure, we draw the graphs of three random walks with respect to the unweighted standard and nonbacktracking random walks. We also generate the eyes on the prize matrix with respect to this adjacency structure. To generate this matrix, we do factor in the distance between each connected pair of points of the lattice. Note that the walks generated by  $F_{i \rightarrow j}^\Gamma$  exhibit concentration around the line  $y = x$ , whereas just three walks with the other matrices cover each edge of the lattice. Though possible, recomputing paths using the adjacency and nonbacktracking matrix does not result in significant qualitative changes from those in Figure 4.

The distribution that we put on the space of correspondences between  $S_i$  and  $S_j$  now immediately follows: we still define it via Equation 2.2, but restrict the support of the distribution to paths in  $\Gamma$  corresponding to paths in  $\tilde{\Gamma}_{ij}$ . The reason for this can be summarized in the following theorem. Before we state it, we require a definition.

**Definition 2.** Let  $P^q \subset M^m$  be a regular submanifold, let  $x_1, \dots, x_q$  be a coordinate chart on  $P$ , and let  $E_{q+1}, \dots, E_m$  be a section of the tangent bundle along  $P$  such that the  $E_j|_P$  are an orthonormal completion of  $T_P P$  in  $T_P M$ . Then the functions  $y_i, 1 \leq i \leq m$  defined by

$$y_i \left( \exp_p \left( \sum_{j=q+1}^m a_j E_j|_p \right) \right) = x_i(p), 1 \leq i \leq q$$

$$y_i \left( \exp_p \left( \sum_{j=q+1}^m a_j E_j|_p \right) \right) = a_i, q+1 \leq i \leq m$$

form a **Fermi normal coordinate chart** with respect to  $P$ .

Fermi normal coordinates, intuitively speaking are the generalization of Cartesian coordinates to a general manifold.

**Theorem 1.** *Let  $x$  and  $y$  be two points in  $M$  with minimizing geodesic  $\gamma$ . Let  $C_{x,y}^\varepsilon$  be the collection of unit speed  $C^1$  curves  $s$  in  $M$  that satisfy the enhanced eyes on the prize conditions*

$$\begin{aligned} g(s'(t), v_{x,s(t)}) &> \varepsilon \\ g(s'(t), v_{s(t),y}) &> \varepsilon \end{aligned}$$

*where  $1 > \varepsilon > 0$  and  $v_{x,s(t)}$  and  $v_{s(t),y}$  are the initial condition vectors for the unit speed geodesic between  $x$  and  $s(t)$ , and  $s(t)$  and  $y$  respectively. Then, given a Fermi coordinate neighborhood of  $\gamma$ , there is a sub-neighborhood such that every path in  $C_{x,y}^\varepsilon$  whose image is contained in the subneighborhood is necessarily a function of the coordinate in the neighborhood corresponding to the geodesic.*

The condition in the above theorem is necessary but by no means sufficient for the eyes on the prize condition between  $x$  and  $y$ . Details are reserved for the appendix. Roughly speaking, the above theorem guarantees that, under reasonable assumptions, unit speed curves can be viewed as a function between two geodesics. Combined with curvature estimates in the appendix, we can obtain a worst case bound as to how much parallel transports along a curve differ from those along a geodesic. Thus, the imposition that the paths supported by our probability measure must satisfy the condition in Definition 2.3 is an attempt to limit the lack of quality of the correspondences.

### 3 Replacing the Minimum Spanning Tree

#### 3.1 Improving Correspondence Quality

As previously stated, the ultimate goal of this work is to replace any reliance on the minimum spanning tree for correspondence consistency. We will ultimately do this by making use of the distribution in the previous section. We now focus on addressing the main reason for the use of the minimum spanning tree: improving quality of automated correspondences.

One of the major challenges faced when computing automated correspondences is the ambiguity as to how to handle pairs of shapes with potentially high levels of geometric difference between homologous areas on two shapes. A specific example of this can be found in Figure ???. In this example, ground-truth correspondence has been established by expert observer-placed landmarks [7]. Note that the area around the yellow landmark for the tooth on the left is a local curvature extrema, whereas the immediate area around



Figure 5: Side profiles of two tooth crowns with homologous landmarks placed by an expert observer; correspondence is given by color. Note in particular the difference in geometry in the areas around the yellow landmark.



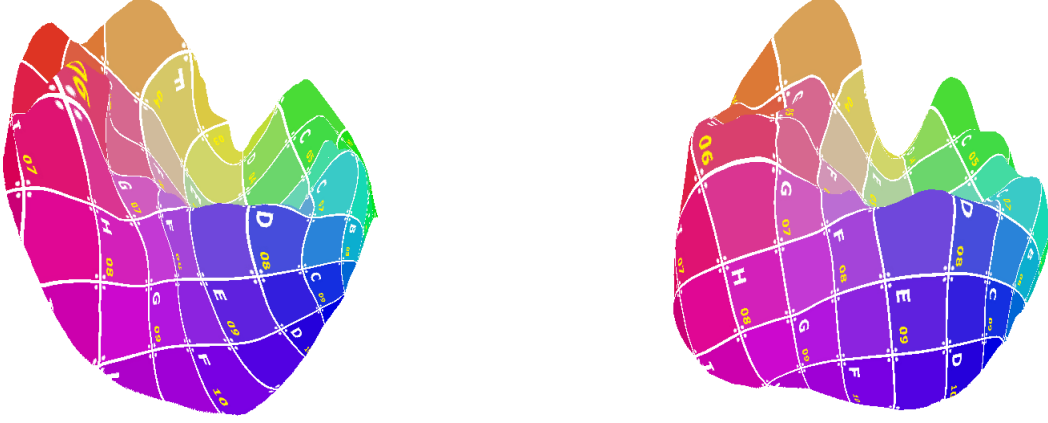


Figure 6: Fully automated texture mapping between two tooth crowns from [7] computed via the algorithm for the continuous Procrustes distance. There is significant discrepancy in correspondence around the pink square with a yellow 6.

the yellow landmark for the right tooth does not appear to satisfy any sort of similar property. This case will create difficulty for many types of automated registration methods due to the asynchronicity in local features. The example in Figure ?? is no exception. Figure 6 shows a computed texture map between these two teeth via the method proposed in [28]. The area around the pink square with the 6 does not match the area suggested by the observer landmark matches in Figure ??, as expected.

As mentioned in the introduction, some recent advances in the fully automated registration procedure make use of an intuitively obvious observation: automated registration is more accurate for objects that are more similar to one another. Here, similarity means low distance, such as the standard and continuous Procrustes distances [28]. Practically, a pair of objects with small distance tend to have the similar geometric features, which makes initial registration of features more accurate. This is where the minimum spanning tree method comes into play: consistency is achieved while this rule of thumb is generally obeyed.

We make an observation key to the computation of continuous maps between surfaces: these maps are generally obtained by interpolating initial sparse correspondences between every pair of teeth, be it physical points or functionals [33]. The mapping implementation used for the continuous Procrustes distance, for example, interpolates sparse correspondences via a thin plate spline. This gives a natural usage of Equations 2.2-2.2: given a point on a surface  $S_i$ , we can use Equations 2.2-2.2 to define a soft correspondence on  $S_j$ . We can then if desired, compute a hard correspondence from the soft correspondence. Care must be made in this process, however, as the distribution is ultimately agnostic to the correctness of the correspondences. As such, we will threshold the distribution by restricting to paths of sufficiently high weight/low energy.

The basic algorithm we use is given in Algorithm 1. We summarize it here. We assume that we have a collection of  $k$  shapes  $S_1, \dots, S_k$ , where the shapes in question can either be point clouds or meshes. We also assume that we have some initially computed maps between the shapes  $f_{nm} : S_m \rightarrow S_n$ , distances  $d_{nm} = d_{mn}$  obtained from these mappings, and some set threshold  $\lambda$ . We iterate through all pairs in the collection. The distances give us a complete graph  $\Gamma$  where each shape is a vertex and each edge has weight  $w_{nm} = w(d_{nm})$ , where  $w$  satisfies  $w(0) = 1$  and some sufficient decay properties for the problem of interest. For every pair of shapes  $S_i$  and  $S_j$ , we compute the matrix  $F_{i \rightarrow j}^\Gamma$ . We then define the weighted version  $WF_{i \rightarrow j}^\Gamma$  given by taking the pointwise Hadamard matrix product of  $W$  with  $F_{i \rightarrow j}^\Gamma$ . The heart of the algorithm lies in a modified depth first search algorithm that iterates over all paths from  $S_i$  to  $S_j$  given by  $WF_{i \rightarrow j}^\Gamma$  and keeps track of both the weight of the path as well as the composed correspondences for each vertex in the shape. The output of this

---

**Algorithm 1** Soft correspondence collection by forward diffusion

---

Input: Shapes  $S_1, \dots, S_k$ ; distances  $(d_{ji})$ ; maps  $\{f_{mn}\}$ ; threshold  $\lambda$   
Compute:  $W := (w_{mn}) = (w(d_{mn}))$   
**for**  $i \in \{1, \dots, k\}$  **do**  
    **for**  $j \in \{1, \dots, k\}$  **do**  
        **if**  $i \neq j$  **then**  
            Compute  $F_{i \rightarrow j}^\Gamma$   
             $WF_{i \rightarrow j}^\Gamma = W \odot F_{i \rightarrow j}^\Gamma$   
             $f_{ji}^s = \text{Modified\_DFS}(\{f_{mn}\}, WF_{i \rightarrow j}^\Gamma, \lambda)$   
             $\bar{f}_{ji} = \text{FrechetMean}(f_{ji}^s)$   
        **end if**  
    **end for**  
**end for**  
Output: Soft correspondences  $\{f_{mn}^s\}$ , Frechet mean correspondences  $\{\bar{f}_{mn}\}$

---

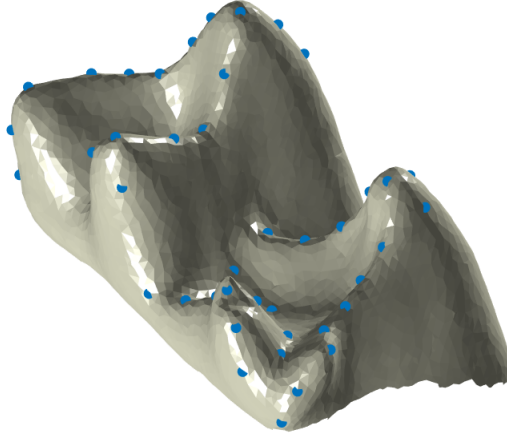


Figure 7: A tooth crown mesh with 50 landmarks selected via a Gaussian Process landmarking procedure

algorithm will yield the soft correspondences with respect to the given distribution, from which, if desired, one can compute a hard correspondence via the Frechet mean or some other statistic.

### 3.1.1 Robust Improvement of Pairwise Correspondences

It is clear that the above algorithm solves the robustness problem while preserving the desirable properties of the minimum spanning tree minus consistency. Whereas the addition or removal of samples of shapes might result in a radical change in the minimum spanning tree (and hence potential volatility in the map), changes in the soft correspondence are much more gradual. It would take a significant amount of maps to introduce a significant change in soft correspondence. By tuning the threshold parameter appropriately, the soft correspondences computed will solely involve compositions of maps between pairs of shapes with high degrees of similarity. Given our interest in interpolating sparse correspondences, we do not in practice make use of every soft correspondence; we will instead utilize the soft correspondences for particular points of interest in our collection. All that is left is to choose features on each surface to match. We propose using Gaussian process landmarks as explained in [30] [17]. These features have a tendency to outline a shape extremely well within a relatively small number of points. Figure 7 gives an example of this for a

tooth crown with approximately 5000 vertices: the first 50 Gaussian process landmarks chosen this way successfully outline a coarse skeleton of the surface.

---

**Algorithm 2** Gaussian Process Landmark Partial Matching

---

```

Input: Shapes  $S_1, S_2$ ; soft correspondences  $f_{12}^s, f_{21}^s$ , Gaussian Process landmarks  $v_1^i, \dots, v_k^i$ , radius  $R$ , distances  $(d_{ji})$ 
Matches = []
for  $i \in \{1, \dots, k\}$  do
  for  $j \in \{1, \dots, k\}$  do
    if  $\mathbb{P}(f_{12}^s(v_i^1) \in \mathcal{A}_{v_j^2}(R)) \geq 0.5$  then
      if  $\mathbb{P}(f_{21}^s(v_j^1) \in \mathcal{A}_{v_i^1}(R)) \geq 0.5$  then
        Matches.append( $j$ )
        BREAK
      end if
    Matches.append(0)
  end if
end for
end for
Output: Matches

```

---

We want to use these features in order to create refined maps. To do this, we use the soft correspondences from Algorithm 1 and employ a partial matching procedure listed in Algorithm 2. For every pair of shapes, we pick some number of Gaussian Process landmarks and some fixed radius  $R$ . The radius allows for some flexibility in the matching procedure; rather than necessitate that the landmarks must correspond exactly, we allow to correspond only approximately. We do allow for discrete radii; in the case of meshes, this would be determined by the underlying connectivity structure

Specifically, let  $\mathcal{A}_{s_m^i}(R)$  be a ball of radius  $R$  about the landmark  $s_m^i$ , where  $R$  and the number of landmarks are chosen so that no balls intersect. We seek to determine the probability that the  $f_{ij}(s_m^i)$  lies within each such ball on the shape  $S_j$ . If this probability is greater than 0.5 for some landmark on  $S_j$ , and the same relation holds vice versa, we deem that the landmarks are in correspondence. We do not admit any landmark correspondences that are not mutual, as such correspondences may lead to texture folding in the interpolation process, as has been observed experimentally with continuous Procrustes maps.

Figure 8 shows a number of examples of pairwise correspondences improved by interpolating the above procedure. The problems with registration are ultimately rooted in the lack of geometric features of each tooth as opposed to traditional computer graphics benchmarks. Tooth crowns do not tend to have as pronounced features as those of a human; in certain cases, areas of the tooth are near flat. This tends to lead to one of three issues with mappings computed: lack of correspondence around low curvature areas, distortion during the mapping procedure, and even lack of convergence to a homeomorphism (not pictured here). In rare cases this can lead to a total mismatch, where the orientation of each tooth is incorrect. By using this partial matching procedure, we can use an entire collection to correct for all of these errors.

### 3.1.2 Accuracy of Ground Truth Propagation

To validate our proposed methods, we test our ability to propagate given ground truth for a collection of anatomical surfaces. We use as data the 116 tooth crowns used in [7]. These teeth are equipped with a consistent set of eighteen observer landmarks divided into two categories: type 2, which correspond to non-geometric features relative to the position of the tooth in the jaw, and type 3 landmarks, which corresponding

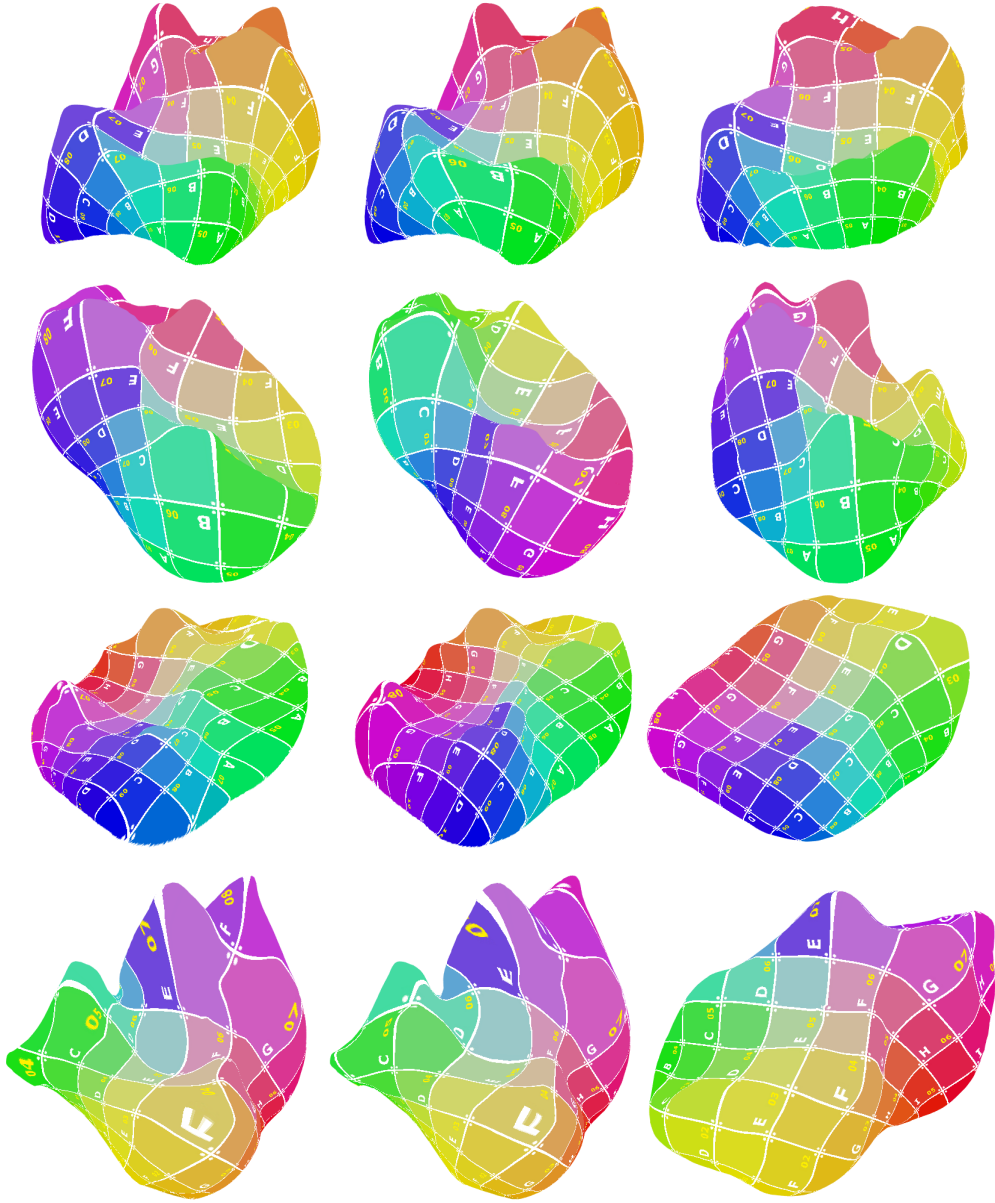


Figure 8: Examples illustrating the ability for interpolation of Gaussian Process partial matching to fix inaccurate correspondences. Right: tooth crown with prescribed texture coordinates. Middle: Computed continuous Procrustes map to the left tooth. Left: Map computed by interpolating Gaussian Process partial matching. From top to bottom: Fixed correspondence of ridges, fixed orientation mismatch, improved matching under featureless teeth, lower distortion for highly different geometries.

to more familiar geometric features such as cusps and saddles. For each surface in the collection, we compute continuous Procrustes distances and the resulting point-to-point maps. We test a number of different ways to propagate landmarks:

- Direct pairwise propagation
- Propagation along a minimum spanning tree
- Frechet mean of the soft correspondences in Algorithm 1 restricted to the support of the distribution
- Maximal likelihood estimate of the soft correspondences in Algorithm 1
- Shortest path propagation after choosing some  $\epsilon$  to compute nearest neighbors.

The first two methods listed are currently utilized and are present to serve as a benchmark as well as to illustrate the general inaccuracies that can occur by solely relying on direct propagation. The next two methods in the list are derived from the algorithms presented above and serve as a test of quality of correspondence in the forward propagation framework. Both of these methods involve a tuning parameter: only admit maps with path weight sufficiently high. Here, the weight between two nodes was given by  $w_{ji} = e^{-d_{ji}^2}$ . The lower threshold for path weight used was .978 and was chosen in an adhoc manner: we visualized the computed correspondences between multiple pairs of shapes of significantly different geometry and tuned appropriately until the computed correspondences were sufficiently accurate. We restricted the Frechet mean computed to the support of the underlying distribution as without that restriction, landmarks could potentially land well outside the support, hence would be nowhere close to being accurate.

The last method makes use of traditional manifold learning assumptions and refines our initial complete graph of shapes and distances by pruning edges between vertices that are of sufficiently high distance from one another as to better approximate our manifold of shapes [4, 34, 41]. We then compute correspondences obtained by following the geodesic of our manifold approximation, and also compute correspondences given by the eyes on the prize walks with respect to this new adjacency structure. We follow the convention of [14, 15] and pick  $\epsilon_D$  such that most pairs of shapes within each genus group are within  $\epsilon_D$  of one another. Any edge with distance higher than  $\epsilon_D$  is removed.

To visualize the accuracy of our method, we utilize the Princeton benchmark introduced in [29]. The axes of this graph are geodesic distance and percentage of computed landmarks that are at most the corresponding geodesic distance away from the ground truth. Each curve on this graph represents the resulting accuracy of the correspondences. We see the results for all pairwise correspondences in Figure 9. We note that the Frechet mean method consistently performed worse on average than the remaining methods. This is not a surprise; as noted in Figure 1, different paths can yield very different correspondences. In the case of the Frechet mean, the distributions observed were disjoint with multiple connected components, allowing for a Frechet mean potentially away from the ground truth correspondence. The other methods, though their results gradated, exhibit similar results. The MST based approach has a lower percentage of low geodesic error correspondences compared to the other three, but as geodesic error increases, the correspondence percentage gets better. Nevertheless, the maximum likelihood estimate consistently outperforms all other methods.

### 3.2 Enforcing Consistency

Though we have successfully demonstrated that the methods from the previous subsection give us the accuracy and robustness desired, we are still left with the problem of enforcing consistency, which is needed for any reasonable statistical application. We would like a method to enforce consistency of mappings that is

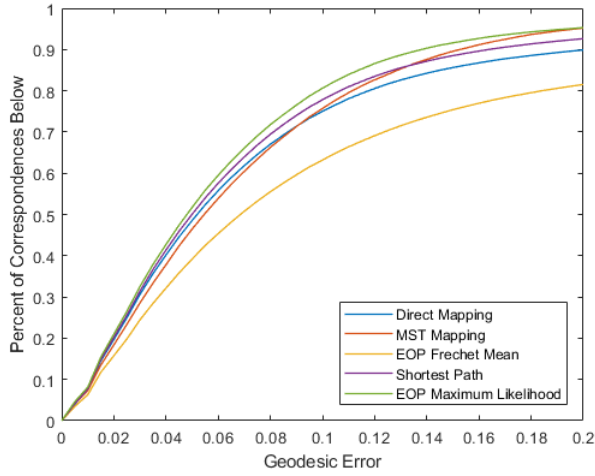


Figure 9: Benchmark for all ground truth correspondences in a collection of 116 teeth.

also ultimately robust to the addition of data. For simplicity, we make use of the Frechet mean shape of the collection with respect to the distance measures, and propose to generate consistent maps for every pair of shapes by first mapping one shape to the Frechet mean, then composing that map with one from the Frechet mean to the other shape in the pair. With a large amount of data, the Frechet mean should only exhibit a minimal amount of fluctuations in the sense that the features of the Frechet mean should remain similar with more data, keeping the proposed procedure stable. Furthermore, by mapping to and from the Frechet mean, we essentially bound the feature disparity between any two surfaces in the mapping process, which will improve the accuracy of pairwise registration.

To test our choice, we also consider the same benchmark in Figure 9 solely on maps to the Frechet mean of the dataset. This can be viewed in Figure 10. We see the same basic pattern established as in Figure 9, although the results for direct propagation, shortest path, and the maximum likelihood estimate are much closer in this case.

We would also like to better understand the effect of our path weight threshold on our resulting analysis, especially concerning our proposed method involving the Frechet mean. To this end, we consider propagations of landmarks to the Frechet mean of the collection via the maximum likelihood estimate above, though we consider multiple path weight thresholds below .978. The results in Figure ?? shows the results of the above benchmark for multiple weights. The results show that there is some degree of robustness to the selection of the lower path weight threshold.



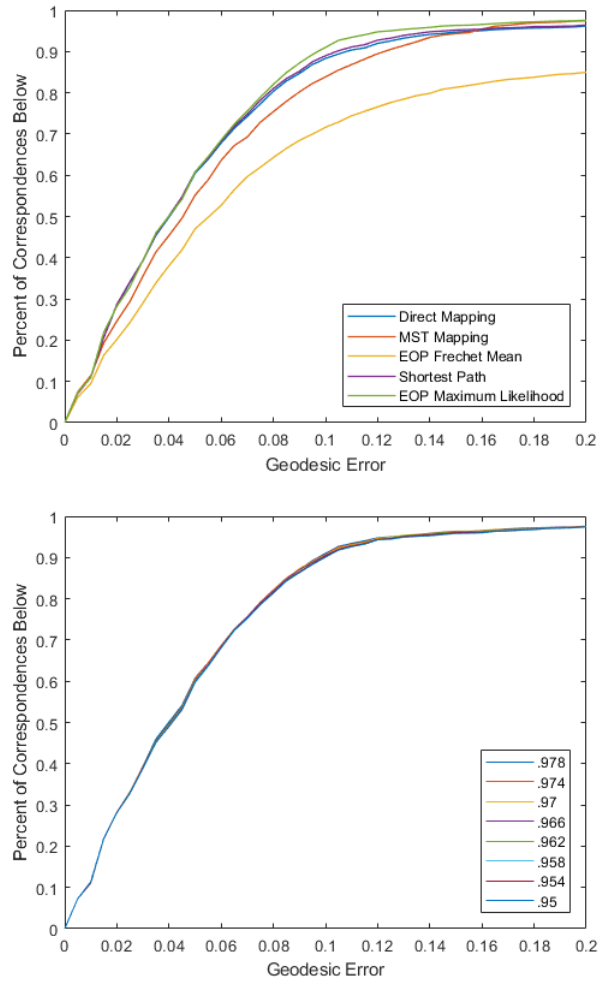


Figure 10: Above: Benchmark for ground truth correspondences mapped to the Frechet mean of a collection of 116 teeth. Below: Benchmark analyzing robustness to change in minimum path weight

## 4 Applications: High Quality Surface Correspondence through Alignment Refinement

As an application of the propagation method in the previous section, we now propose a way to obtain consistent, high-quality, almost fully-automated registration of homeomorphic surfaces provided that the surfaces are all consistently aligned. The basic idea is that, for surfaces that are reasonably similar to one another, most of the correct correspondence can be obtained by looking solely at the alignment. It might not be sufficient, however, to determine the registration solely by projection following the alignment. If we are interested in correspondences that are functional in nature, i.e. matching curvature extremas, then it is possible that some of the curvature extremas will not be in perfect alignment, and the map determined by the alignment will not map the curvature extrema to one another despite their obvious correspondence.

---

### Algorithm 3 Obtaining Mappings by Revising Alignments

---

Input: Aligned shapes  $S_1, S_2$ ; soft correspondences  $f_{12}^s, f_{21}^s$ , Gaussian Process landmarks  $v_1^i, \dots, v_k^i$ , radius  $R$ , curvature distance tolerance  $\delta$ , connected shape graph  $\Gamma$

Matches = []

**for**  $i \in \{1, \dots, k\}$  **do**

    Compute curvature extrema  $\{v_i^m\} \subset S_i$

    Extract  $n$  Gaussian process landmarks  $\{v_i^j\} \subset S_i$

**end for**

**for**  $i \in \{1, \dots, k\}$  **do**

**for**  $j \in \{1, \dots, k\}$  **do**

        Compute projection of  $v_i^{m_i}$  on  $S_j$ ,  $P_{ji}v_i^m$ , and projection of  $v_j^m$ .  $P_{ij}v_j^{m_j}$  on  $S_i$

        PossibleCurvatureMatches =  $\{(v_i^{m_i}, v_j^{m_j}) : d_{S_i}(P_{ji}v_i^m, \{v_j^{m_j}\}) < \delta\}$

        CurvatureMatches = StableMatching(PossibleCurvatureMatches)

        PartialMatches = GPPartialMatching( $S_i, S_j$ )

**end for**

**end for**

$f$  = index of base shape

**for**  $i \in \{1, \dots, k\}$  **do**

**if**  $i \neq f$  **then**

        CurMatches = CurvatureMatches $\{i, f\}$

**while** size(CurMatches)  $\neq$  maxMatches **do**

            CurMatches.append( $\operatorname{argmax}_{(v_i, v_j) \in \text{PartialMatches}} d_{S_i}(\text{CurMatches}_i, v_i) + d_{S_j}(\text{CurMatches}_j, v_j)$ )

**end while**

**end if**

    Matches.append {CurMatches}

**end for**

Interpolate(Correspondences)

Output: Correspondences

---

We refer to Algorithm 3 for specific details. The idea is as follows. After alignment, we select some subset of curvature extrema on each shape and compute them. We then compute, for each pair of shapes, the image of each shape’s curvature extrema onto the other via nearest neighbors. Note that the curvature extrema need not map this way to another curvature extrema. We compute, however, the distance of each image of a curvature extrema on one shape to the curvature extrema on the target shape. If there is at least one extrema on the target shape within a sufficient distance to the image of a mapped extrema, and

vice versa, then the two features are matched to one another. In the situation where there an extrema has multiple candidate matches satisfying this criterion, we propose following the Gale-Shapely stable matching procedure, ranking preference of a given matching by minimal distances in the target shape [12]. Ties are assumed to be broken arbitrarily. Note that we have not encountered a case where the stable-matching procedure had to be used in practice.

After the curvature matches are computed, we attempt to match the rest of the shape using Algorithm 2. Distances are calculated using the standard Procrustes distance on subsampled shapes, which can be computed using the Auto3DGM framework [8]. The radius used for the matching process needs to be chosen conservatively to guarantee matching of features that do not over on one another. After this procedure, we have two sets of landmark matching: those obtained by the curvature extrema matching, and those obtained by Algorithm 2. It is possible that the landmark matchings are not consistent to one another; this can occur if homologous curvature extrema are not fully overlapping in the alignment, and one of the extrema maps to some other chosen landmark and vice versa. We thus distill the total set of sparse correspondences to a smaller set as follows: we keep all of the curvature-based landmark matches, and then iteratively add matches made via Algorithm 2 by selecting matches that maximize the joint farthest point sampling energy, i.e. if  $B$  is the initial set of possibly overlapping landmarks and  $A^k := \{(A_i^k, A_j^k)\}$ , is the refined collection of landmarks at iteration  $k$ , we have

$$A^{k+1} = A^k \cup \left\{ \operatorname{argmax}_{(v_i, v_j) \in B \cap (A^k)^c} d_{S_i}(A_i^k, v_i) + d_{S_j}(A_j^k, v_j) \right\}$$

where  $d_{S_k}$  is the geodesic distance on  $S_k$ . We terminate this algorithm after we obtain some preset number of desired correspondences, which will depend on the shapes of interest. We can then obtain these maps by interpolating this collection of sparse correspondences. There are many ways to do this depending on shape topology and data structure. Given that we need correspondences that are consistent, we again choose some shape as the base for which to construct the mappings as in the previous section. In practice, we again make use of the Frechet mean with respect to the shape distances computed from alignment.

We display the results of our algorithm on 24 ankle bones of primates in Figure 11. These shapes represent a simple yet useful real-world case of mapping. Though all of the shapes are geometrically similar, there are significant enough differences in the exact location of the magenta areas (known as the lateral plantar tubercles) which create difficulty when trying to obtain correspondence purely through alignment. In this example, we extract local maxima of the conformal factor obtained by uniformizing each surface to a sphere via the algorithm in [11]. From this, we follow the partial correspondence procedure and Algorithm 3 to obtain 15 landmarks for each shape to the Frechet mean, which we then interpolate via [1]. The surfaces were all reparametrized to the Frechet mean, resulting in every vertex on every shape being in perfect correspondence with some other vertex on every other shape. Our results show successful registration of areas that are functionally in correspondence.

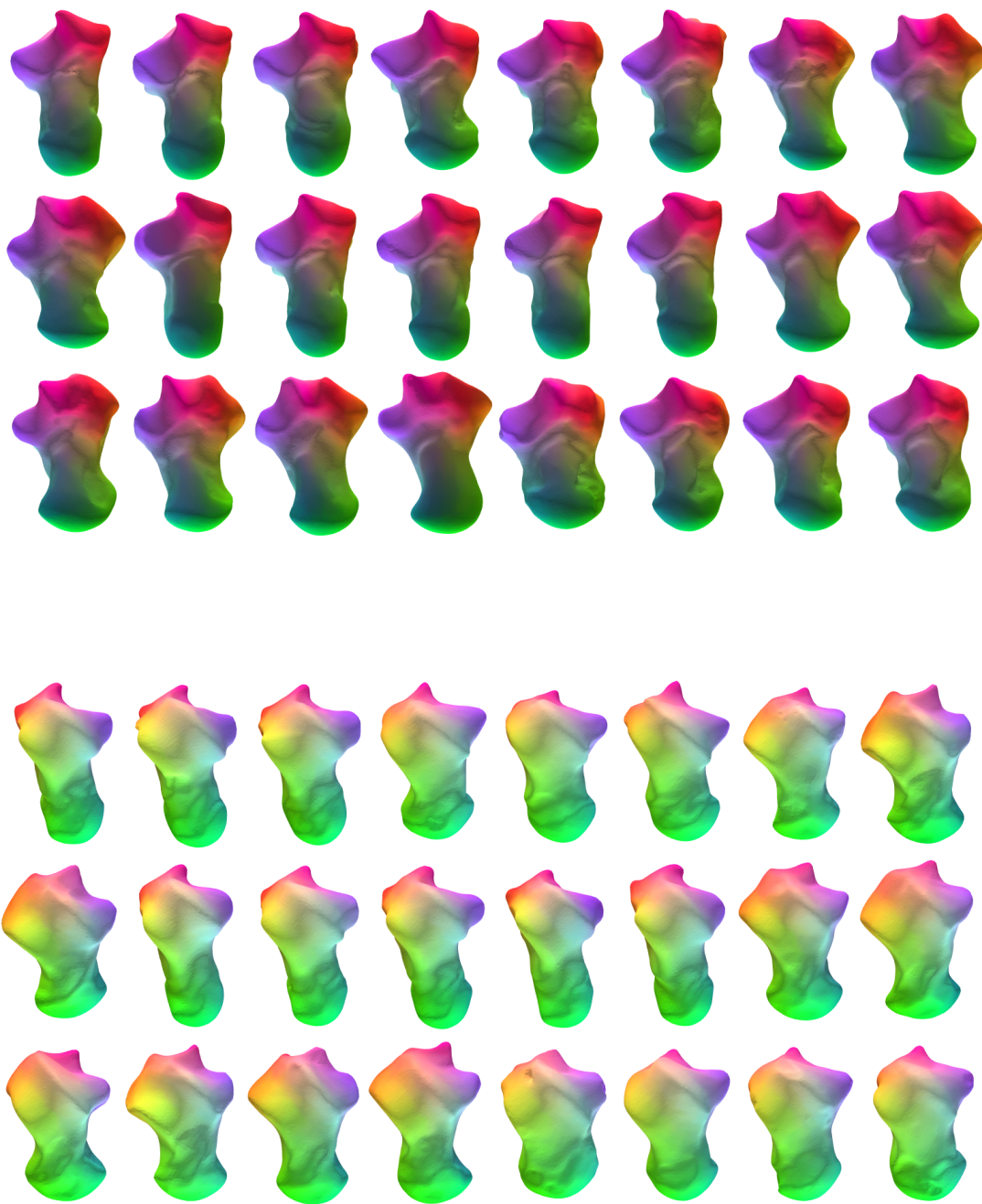


Figure 11: Two profiles of twenty four consistently registered talus bones. Vertices of the same color are in correspondence.

## 5 Conclusion

There are numerous avenues of interest to extend this work. From a theoretical perspective, there are interesting parallels with our proposed method and Brownian bridges, i.e. Brownian motion between two set points. In particular, the soft correspondences in Algorithm 1 is a distribution generated by sampled paths satisfying the speed criterion in Definition 2.3. It would be particularly interesting to, given the framework in [15] and its relation here, investigate Brownian bridges on fibre bundles, where we specifically focus on building a bridge on the *base manifold* and not just the total manifold.

From a practical perspective, there are still many ways that one could improve this method. Though we essentially used Algorithm 1 to propagate delta functions from one shape to another, there is nothing preventing one from doing the same with other distributions. In particular, propagation of indicator functions of areas of high curvature proved to be vital experiments in the process of writing this paper. It would be extremely interesting to investigate the potential for propagating other distributions via this framework, particularly investigating if there is any particular link between the framework mentioned here and functional maps.

Our choice of using the Frechet mean, while simple and intuitive, is not completely effective for all surface matching problems. Issues may still exist if attempting to register a feature-rich shape with one that is feature-less. It would be interesting to adapt the ideas of this work to grow a tree or develop a new algorithm that would guarantee consistency of mappings.

### 5.1 Acknowledgements

Robert Ravier would like to thank AFOSR for funding the work of this article via the NDSEG Fellowship.

## References

- [1] N. Aigerman and Y. Lipman. Hyperbolic orbifold tutte embeddings. *ACM Trans. Graph.*, 35(6):217–1, 2016.
- [2] N. Aigerman, R. Poranne, and Y. Lipman. Seamless surface mappings. *ACM Transactions on Graphics (TOG)*, 34(4):72, 2015.
- [3] A. S. Bandeira, N. Boumal, and A. Singer. Tightness of the maximum likelihood semidefinite relaxation for angular synchronization. *Mathematical Programming*, pages 1–23.
- [4] M. Belkin and P. Niyogi. Laplacian eigenmaps for dimensionality reduction and data representation. *Neural computation*, 15(6):1373–1396, 2003.
- [5] C. Bordenave, M. Lelarge, and L. Massoulié. Non-backtracking spectrum of random graphs: community detection and non-regular ramanujan graphs. In *Foundations of Computer Science (FOCS), 2015 IEEE 56th Annual Symposium on*, pages 1347–1357. IEEE, 2015.
- [6] J.-P. Bourguignon and H. Karcher. Curvature operators: pinching estimates and geometric examples. 1978.
- [7] D. M. Boyer, Y. Lipman, E. S. Clair, J. Puente, B. A. Patel, T. Funkhouser, J. Jernvall, and I. Daubechies. Algorithms to automatically quantify the geometric similarity of anatomical surfaces. *Proceedings of the National Academy of Sciences*, 108(45):18221–18226, 2011.

- [8] D. M. Boyer, J. Puente, J. T. Gladman, C. Glynn, S. Mukherjee, G. S. Yapuncich, and I. Daubechies. A new fully automated approach for aligning and comparing shapes. *The Anatomical Record*, 298(1):249–276, 2015.
- [9] K. N. Chaudhury, Y. Khoo, and A. Singer. Global registration of multiple point clouds using semidefinite programming. *SIAM Journal on Optimization*, 25(1):468–501, 2015.
- [10] I. Chavel. *Riemannian geometry: a modern introduction*, volume 98. Cambridge university press, 2006.
- [11] P. T. Choi, K. C. Lam, and L. M. Lui. Flash: Fast landmark aligned spherical harmonic parameterization for genus-0 closed brain surfaces. *SIAM Journal on Imaging Sciences*, 8(1):67–94, 2015.
- [12] L. E. Dubins and D. A. Freedman. Machiavelli and the gale-shapley algorithm. *The American Mathematical Monthly*, 88(7):485–494, 1981.
- [13] N. Dym and Y. Lipman. Exact recovery with symmetries for procrustes matching. *arXiv preprint arXiv:1606.01548*, 2016.
- [14] T. Gao. *Hypoelliptic Diffusion Maps and Their Applications in Automated Geometric Morphometrics*. PhD thesis, Citeseer, 2015.
- [15] T. Gao. The diffusion geometry of fibre bundles. *arXiv preprint arXiv:1602.02330*, 2016.
- [16] T. Gao, J. Brodzki, and S. Mukherjee. The geometry of synchronization problems and learning group actions. *arXiv preprint arXiv:1610.09051*, 2016.
- [17] T. Gao, S. Z. Kovalsky, D. M. Boyer, and I. Daubechies. Gaussian process landmarking on manifolds. *arXiv preprint arXiv:1802.03479*, 2018.
- [18] T. Gao, G. S. Yapuncich, I. Daubechies, S. Mukherjee, and D. M. Boyer. Development and assessment of fully automated and globally transitive geometric morphometric methods, with application to a biological comparative dataset with high interspecific variation. *bioRxiv*, page 086280, 2016.
- [19] L. Gulikers, M. Lelarge, and L. Massoulié. Non-backtracking spectrum of degree-corrected stochastic block models. *arXiv preprint arXiv:1609.02487*, 2016.
- [20] Q.-X. Huang and L. Guibas. Consistent shape maps via semidefinite programming. In *Computer Graphics Forum*, volume 32, pages 177–186. Wiley Online Library, 2013.
- [21] Q.-X. Huang, G.-X. Zhang, L. Gao, S.-M. Hu, A. Butscher, and L. Guibas. An optimization approach for extracting and encoding consistent maps in a shape collection. *ACM Transactions on Graphics (TOG)*, 31(6):167, 2012.
- [22] D. F. Huber. *Automatic three-dimensional modeling from reality*. PhD thesis, 2002.
- [23] C. Intanagonwiwat, R. Govindan, D. Estrin, J. Heidemann, and F. Silva. Directed diffusion for wireless sensor networking. *IEEE/ACM Transactions on Networking (ToN)*, 11(1):2–16, 2003.
- [24] I. H. Jermyn, S. Kurtek, E. Klassen, and A. Srivastava. Elastic shape matching of parameterized surfaces using square root normal fields. In *European conference on computer vision*, pages 804–817. Springer, 2012.



- [25] I. Kezurer, S. Z. Kovalsky, R. Basri, and Y. Lipman. Tight relaxation of quadratic matching. In *Computer Graphics Forum*, volume 34, pages 115–128. Wiley Online Library, 2015.
- [26] V. G. Kim, Y. Lipman, and T. Funkhouser. Blended intrinsic maps. In *ACM Transactions on Graphics (TOG)*, volume 30, page 79. ACM, 2011.
- [27] J. M. Lee. *Riemannian manifolds: an introduction to curvature*, volume 176. Springer Science & Business Media, 2006.
- [28] R. Lipman, Yaron and Al-Aifari and I. Daubechies. Continuous procrustes distance between two surfaces. *Communications on Pure and Applied Mathematics*, 66(6):934–964, 2013.
- [29] Y. Lipman and T. Funkhouser. Möbius voting for surface correspondence. In *ACM Transactions on Graphics (TOG)*, volume 28, page 72. ACM, 2009.
- [30] A. C. Öztireli, M. Alexa, and M. Gross. Spectral sampling of manifolds. *ACM Transactions on Graphics (TOG)*, 29(6):168, 2010.
- [31] P. Petersen, S. Axler, and K. Ribet. *Riemannian geometry*, volume 171. Springer, 2006.
- [32] J. Puente. Distances and algorithms to compare sets of shapes for automated biological morphometrics. 2013.
- [33] E. Rodolà, L. Cosmo, M. M. Bronstein, A. Torsello, and D. Cremers. Partial functional correspondence. In *Computer Graphics Forum*, volume 36, pages 222–236. Wiley Online Library, 2017.
- [34] S. T. Roweis and L. K. Saul. Nonlinear dimensionality reduction by locally linear embedding. *science*, 290(5500):2323–2326, 2000.
- [35] A. Saade, F. Krzakala, and L. Zdeborová. Spectral density of the non-backtracking operator on random graphs. *EPL (Europhysics Letters)*, 107(5):50005, 2014.
- [36] R. Shi, W. Zeng, Z. Su, J. Jiang, H. Damasio, Z. Lu, Y. Wang, S.-T. Yau, and X. Gu. Hyperbolic harmonic mapping for surface registration. *IEEE transactions on pattern analysis and machine intelligence*, 39(5):965–980, 2017.
- [37] A. Singer. Angular synchronization by eigenvectors and semidefinite programming. *Applied and computational harmonic analysis*, 30(1):20–36, 2011.
- [38] S. Sodin. Random matrices, nonbacktracking walks, and orthogonal polynomials. *Journal of Mathematical Physics*, 48(12):123503, 2007.
- [39] J. Solomon, A. Nguyen, A. Butscher, M. Ben-Chen, and L. Guibas. Soft maps between surfaces. In *Computer Graphics Forum*, volume 31, pages 1617–1626. Wiley Online Library, 2012.
- [40] M. Styner, I. Oguz, S. Xu, C. Brechbühler, D. Pantazis, J. J. Levitt, M. E. Shenton, and G. Gerig. Framework for the statistical shape analysis of brain structures using spharm-pdm. *The insight journal*, (1071):242, 2006.
- [41] J. B. Tenenbaum, V. De Silva, and J. C. Langford. A global geometric framework for nonlinear dimensionality reduction. *science*, 290(5500):2319–2323, 2000.
- [42] N. S. Vitek, C. L. Manz, T. Gao, J. I. Bloch, S. G. Strait, and D. M. Boyer. Semi-supervised determination of pseudocryptic morphotypes using observer-free characterizations of anatomical alignment and shape. *Ecology and Evolution*, 2017.

## A Technical Details

### A.1 A Quick Review of Connections, Curvature Parallel Transport

We briefly review major relevant concepts from Riemannian Geometry, but make no attempt to summarize everything. We let  $(M^m, g)$  be an  $m$ -dimensional Riemannian manifold with metric  $g$ . Readers unfamiliar with notions of Riemannian geometry may find more information about these ideas, as well as the ones below, in standard textbooks [27, 31]. We specifically focus on tangent bundles. We let  $\mathcal{V}(M)$  denote the space of smooth vector fields on  $M$ .

**Definition 3.** A **connection** on  $M$  is a map  $\nabla : \mathcal{V}(M) \times \mathcal{V}(M) \rightarrow \mathcal{V}(M)$ , written  $(X, Y) \rightarrow \nabla_X Y$ , that satisfies the following three properties:

1. For  $f, g$  smooth functions on  $M$  and  $X, Y, Z$  smooth vector fields, we have

$$\nabla_{fX+gY}Z = f\nabla_X Z + g\nabla_Y Z$$

2. For  $a, b \in \mathbb{R}$  and  $X, Y, Z$  smooth vector fields on  $M$ , we have

$$\nabla_X(aY + bZ) = a\nabla_X Y + b\nabla_X Z$$

3. For  $f$  a smooth function on  $M$  and  $X, Y$  smooth vector fields, we have a Leibniz rule

$$\nabla_X(fY) = f\nabla_X Y + (Xf)Y$$

where  $X$  acts a partial derivative on  $f$

Connections are the appropriate analogue of a directional derivative for vector fields. Specifically, for a vector field  $X$  along a curve  $\gamma : [a, b] \rightarrow M$ ,  $X'(t) = \frac{d}{dt}X := \nabla_{\dot{\gamma}(t)}X$ , sometimes written as  $\nabla_{\frac{d}{dt}}X$ . It is well-known in Riemannian geometry that every manifold has a unique connection called the **Levi-Civita connection** that satisfies the above as well as two additional properties: it is symmetric, i.e.

$$\nabla_X Y - \nabla_Y X = [X, Y]$$

where  $[\cdot, \cdot]$  is the Lie bracket on  $TM$ , the tangent bundle of  $M$ , and it is compatible with the metric, i.e.

$$\nabla_X g(Y, Z) = g(\nabla_X Y, Z) + g(X, \nabla_Y Z)$$

The Levi-Civita connection satisfies the following property, which only explicitly requires that the connection be compatible.

**Lemma 1.** Let  $X(t)$  be a smooth vector field defined along a curve  $\gamma : [a, b] \rightarrow M$  nowhere equal to zero. Then we have

$$\frac{d}{dt}\|X\| := \frac{d}{dt}(g(X, X))^{\frac{1}{2}} \leq (g(X, X))^{\frac{1}{2}} = \|\nabla_{\frac{d}{dt}}X\|$$

where all derivatives are taken with respect to the Levi-Civita connection.

*Proof.* Since the Levi-Civita connection is symmetric, we have

$$\begin{aligned}\frac{d}{dt}(g(X, X))^{\frac{1}{2}} &= \frac{1}{2}g(X, X)^{-\frac{1}{2}} \frac{d}{dt}g(X, X) \\ &= \frac{1}{2}g(X, X)^{-\frac{1}{2}} 2g(\nabla_{\frac{d}{dt}} X, X) \\ &= g(X, X)^{-\frac{1}{2}} g(\nabla_{\frac{d}{dt}} X, X)\end{aligned}$$

by symmetry of the Riemannian metric and compatibility of the Levi-Civita connection. A direct application of the Cauchy-Schwarz inequality on  $g(X', X)$  completes the proof.  $\square$

Here on out, we assume that  $\nabla$  is the Levi-Civita connection on  $M$ . The following definition lies at the heart of our reasoning in Chapter 2. It does not strictly require the Levi-Civita connection, but we will only use it in this case.

**Definition 4.** Let  $\gamma : [a, b] \rightarrow M$  be a smooth curve and let  $v \in T_{\gamma(a)}M$ . The **parallel transport** of  $v$  with respect to  $\gamma$  is the unique vector field  $V(t) \in T_{\gamma(t)}M$  such that

$$\begin{aligned}V(a) &= v \\ \nabla_{\dot{\gamma}(t)} V(t) &= 0\end{aligned}$$

The above equation does have an expansion in local coordinates, but this is not required for our purposes. We can then define an operator  $P_{y,x}^\gamma : T_x M \rightarrow T_y M$  by parallel transporting every vector in  $T_x M$  to  $T_y M$  along  $\gamma$ . This is in general an isomorphism of vector spaces, and, with respect to the Levi-Civita connection, an isometry.

In order to properly discuss parallel transport, we also need the manifold notion of curvature.

**Definition 5.** The **Riemann curvature tensor**  $R(X, Y)Z$ , where each argument is a vector field, is defined by

$$R(X, Y)Z = \nabla_X \nabla_Y Z - \nabla_Y \nabla_X Z - \nabla_{[X, Y]} Z$$

In particular, note that the last term in the above definition drops out in the case that  $X$  and  $Y$  are coordinate vector fields.

## A.2 Clarifying Thoughts on Curvature

The particular interest in Theorem 2.3, as alluded to in Section 2 is in the following result, which is an exercise in [10].

**Theorem 2.** Let  $H(s, t)$  be a homotopy between two smooth curves  $\gamma_0(t) := H(0, t)$  and  $\gamma_1(t) := H(1, t)$  that do not intersect except at endpoints  $p := H(s, 0)$  and  $q := H(s, 1)$ . Let  $X \in T_p M$  be a unit vector, and let  $X_s$  be the vector field defined by parallel transporting  $X$  along  $\gamma_s(t) := H(s, t)$  for  $s$  fixed. Then

$$\|X_1(1) - X_0(1)\| \leq \frac{4}{3} K_{\max} A(H)$$

where  $A(H)$  is the area of the graph of the homotopy and  $K_{\max}$  is the maximum of the absolute Gaussian curvature of the graph of the homotopy.

The above estimate gives a bound on the deviation of the parallel transport between two curves. From a manifold learning perspective, we cannot necessarily control the sectional curvatures of the manifold of interest. However, depending on the data, we may be able to control the properties of the paths between every pair of points used. This is where the previous proposition comes into play. So long as paths move sufficiently quickly from the source point to the target point, they can be described as functions of the geodesic between those two points. As functions of the geodesic, there is a natural homotopy between each such path and the geodesic. For all such sufficiently smooth paths, we can then find the worst case area by solving a variational problem assuming that the length of the path in question is some constant. This establishes the alluded-to bounding of path quality

*Proof.* By the fundamental theorem of calculus, we have

$$\begin{aligned}\|X_1(1) - X_0(1)\| &= \left\| \int_0^1 \nabla_{\frac{d}{ds}} X_s(1) ds \right\| \\ &\leq \int_0^1 \|\nabla_{\frac{d}{ds}}(X_s(1))\| ds \\ &= \int_0^1 \left( \|\nabla_{\frac{d}{ds}}(X_s(1))\| - \|\nabla_{\frac{d}{ds}} X_s(0)\| \right) ds\end{aligned}$$

where the last equality follows from the assumption that  $X_s(0)$  is constant. Another application of the fundamental theorem gives

$$\begin{aligned}\|X_1(1) - X_0(1)\| &\leq \int_0^1 \left( \|\nabla_{\frac{d}{ds}}(X_s(1))\| - \|\nabla_{\frac{d}{ds}} X_s(0)\| \right) ds \\ &= \int_0^1 \left( \int_0^1 \frac{d}{dt} \|\nabla_{\frac{d}{ds}}(X_s(t))\| dt \right) ds \\ &\leq \int_0^1 \left( \int_0^1 \|\nabla_{\frac{d}{dt}} \nabla_{\frac{d}{ds}}(X_s(t))\| dt \right) ds \\ &= \int_0^1 \left( \int_0^1 \|(\nabla_{\frac{d}{dt}} \nabla_{\frac{d}{ds}} - \nabla_{\frac{d}{ds}} \nabla_{\frac{d}{dt}})(X_s(t))\| dt \right) ds\end{aligned}$$

where the second inequality follows from Lemma 1 and the last equality follows from the definition of parallel transport. Since  $\frac{d}{ds}$  and  $\frac{d}{dt}$  are coordinate vector fields, we have from Definition 5

$$\|X_1(1) - X_0(1)\| \leq \int_0^1 \left( \int_0^1 \|R(H_t, H_s)(X_s(t))\| dt \right) ds$$

where  $H_t$  and  $H_s$  are the corresponding partial derivative vector fields of the homotopy  $H$ . The Riemann curvature term in the above integral is bounded above by  $\frac{4}{3} K_{max} \|H_s \wedge H_t\|$ , where  $\|H_s \wedge H_t\|$  is the induced area form of the homotopy; this is a direct consequence of Lemma 3.7 in [6]. The desired result immediately follows.  $\square$

## B Proof of Theorem 2.3

Assume that the inner products of  $s'(t)$  with  $v_{s(t),x}$  and  $v_{s(t),y}$  are strictly bounded above and below respectively by some uniform numbers  $M_1$  and  $M_2$  whenever the inner products are well defined, i.e. when

$s(t) \neq x, y$ . We now define two sets: let  $U_{x,\varepsilon}$  be the subset of  $M$  such that every point  $u \in U_{x,\varepsilon}$  satisfies  $g\left(v_{x,u}, \frac{\partial}{\partial \gamma}\right) \geq 1 - \varepsilon$ , and analogously  $U_{y,\varepsilon}$ . If  $M_1$  and  $M_2$  are at least  $\varepsilon$ , then any such curve  $s(t)$  contained in the intersection of the Fermi coordinate neighborhood of  $\gamma$  with the union of  $U_{x,\varepsilon}$  and  $U_{y,\varepsilon}$  necessarily has to satisfy  $g\left(s'(t), \frac{\partial}{\partial \gamma}\right) > 0$ . An application of the implicit function theorem then completes the proof.

**Remark 1.** *The assumption that the inner products are lower bounded by some fixed constant can be removed in the Euclidean case to simply being positive. The proof then follows from the law of cosines. This method fails to generalize for other manifolds as curvature affects possible angles of intersections for triangles.*